Ultrasonics - Sonochemistry 42 (2018) 48–56

Contents lists available at ScienceDirect

Ultrasonics - Sonochemistry

journal homepage: www.elsevier.com/locate/ultson

Correlating ultrasonic impulse and addition of ZnO promoter with CO_2 conversion and methanol selectivity of CuO/ZrO_2 catalysts

Collins I. Ezeh[a,c], Xiaogang Yang[b,c,*], Jun He[a,c,*], Colin Snape[d], Xiao Min Cheng[e]

[a] Department of Chemical and Environmental Engineering, University of Nottingham Ningbo China, University Park, Ningbo 315100 PR China
[b] Department of Mechanical, Materials and Manufacturing Engineering, University of Nottingham Ningbo China, University Park, Ningbo 315100 PR China
[c] International Doctoral Innovation Centre, University of Nottingham Ningbo China, University Park, Ningbo 315100 PR China
[d] Department of Chemical and Environmental Engineering, University of Nottingham, University Park, Nottingham NG7 2RD, UK
[e] Department of Mechanical, Materials and Manufacturing Engineering, Ningbo University of Technology, Jiangbei District, Ningbo, Zhejiang 315211 PR China

ARTICLE INFO

Keywords:
Carbon dioxide
Thermal stability
Hydrogenation
Catalysts
Methanol synthesis

ABSTRACT

The thermal characteristics of Cu-based catalysts for CO_2 utilization towards the synthesis of methanol were analysed and discussed in this study. The preparation process were varied by adopting ultrasonic irradiation at various impulses for the co-precipitation route and also, by introducing ZnO promoters using the solid-state reaction route. Prepared catalysts were characterised using XRD, TPR, TPD, SEM, BET and TG-DTA-DSC. In addition, the CO_2 conversion and CH_3OH selectivity of these samples were assessed. Calcination of the catalysts facilitated the interaction of the Cu catalyst with the respective support bolstering the thermal stability of the catalysts. The characterisation analysis clearly reveals that the thermal performance of the catalysts was directly related to the sonication impulse and heating rate. Surface morphology and chemistry was enhanced with the aid of sonication and introduction of promoters. However, the impact of the promoter outweighs that of the sonication process. CO_2 conversion and methanol selectivity showed a significant improvement with a 270% increase in methanol yield.

1. Introduction

Present research undertaking towards methanol synthesis has been aimed at developing catalysts with great catalytic activity. One notable catalyst for this purpose is the alumina (Al_2O_3) based catalyst with good yield of methanol. However, this catalyst is limited in performance due to its strong hydrophilic characteristics [1–3]. Other catalysts used are Cu-ZrO_2 based catalysts with high thermal stability and Cu dispersion. This is due to the role of ZrO_2 in enhancing catalyst stability and active sites [3,4]. As a result, the catalytic capacity of this material was observed to increase. Further improvement with the dispersion of Cu in this material was achieved by the use of promoters like oxides of Mg [5–7], Mn [5,7,8], Ga [7] and Zn [9,10].

Despite the composition of the catalyst, other means of promoting the performance of the catalyst is the adopted synthetic method and conditions [7,11–13]. Common synthetic methods used for the preparation of these compounds are co-precipitation [3,4,11,12,14–20], sol gel [21,22] and citrate thermal decomposition [7,19,20,23]. Recently, new synthetic methods are being proposed. This includes solid-state chemical reactions [24] and solution combustion [25,26]. Nonetheless, these methods produce materials with low surface area, which is a demerit for catalytic activity [27–31]. To this effect, incorporating ultrasonic irradiation has shown to improve surface area and chemistry [32,33]. Sonication alters particle morphology and it depends on various factors like sonication time and frequency [34,35]. In addition, it can be stipulated that particle morphology also depends on sonication impulse time [34,36].

In this work, CuO-ZrO_2 composite oxide was synthesised via ultrasonic enhanced co-precipitation method with varying impulse time. In addition, the use of ZnO promoter was also used to study the promotional effect of ZnO on CuO-ZrO_2 catalyst. The structural and textural characteristics of these compounds were assessed to study the impact of ultrasonic impulse time and Zn^{2+} introduction on the catalysts morphology and surface chemistry. In addition, a catalytic performance test was conducted to evaluate methanol selectivity and CO_2 conversion of the prepared catalyst.

* Corresponding authors at: Department of Mechanical, Materials and Manufacturing Engineering, University of Nottingham Ningbo China, University Park, Ningbo 315100 PR China (X. Yang). Department of Chemical and Environmental Engineering, University of Nottingham Ningbo China, University Park, Ningbo 315100 PR China (J. He).
E-mail addresses: Xiaogang.Yang@nottingham.edu.cn (X. Yang), jun.he@nottingham.edu.cn (J. He).

https://doi.org/10.1016/j.ultsonch.2017.11.013
Received 2 August 2017; Received in revised form 7 November 2017; Accepted 8 November 2017
Available online 08 November 2017
1350-4177/

2. Experimental

2.1. Material preparation

In this study, the catalysts were synthesised by the ultrasonic aided co-precipitation method. All chemicals used for experimentation were acquired from SinoPharm Chemical Reagents Co. Ltd.

2.2. Preparation of catalyst

2.2.1. Cu/ZrO_2

The catalyst was prepared by a reaction of 0.17 M mixed reaction of $Zr(NO_3)_4$ and $Cu(NO_3)_2$ (Cu-loading = 30%) and 0.1 M NaOH solution while sustaining the pH at 7.0. Mixing was done with the aid of ultrasonic irradiation at different impulse time (continuous, 1, 4 and 8 s). These impulses are chosen to determine appreciable differences in surface morphology around the traditional continuous irradiation which has no impulse time (0 s). After which, the precipitates were filtered, washed, dried (383 K for 6 h) and calcined (at temperature of 623 K for 4 h). This sample is labelled as CZr.

2.2.2. $Cu/Zn/ZrO_2$

A mix of $Cu(NO_3)_2{\cdot}3H_2O$, $Zn(NO_3)_2{\cdot}6H_2O$ and $Zr(NO_3)_4{\cdot}5H_2O$ were blended in a Cu^{2+}:Zn^{2+}:Zr^{4+} molar ratio of 3:1:6. This mix was further blended with citric acid ligand, $C_6H_8O_7{\cdot}H_2O$ in a molar ratio of 1:1.3 [24]. This was carried out for 30 min in an ultrasonic bath at room temperature until the reactants were transformed to a homogeneous muddy precursor. Afterwards, the catalyst was dried at 383 K for 6 h before being calcined at a temperature of 623 K for 4 h. This sample is labelled as CZZr-316. The effect of Zn^{2+} on the catalyst was studied by varying the composition of Zn^{2+} in the catalyst while keeping the composition of Cu^{2+} constant. Given that the suitable Cu-loading for optimum methanol synthesis through hydrogenation for the CZr catalyst is 30%, Cu^{2+} content was restricted to this value with the introduction of Zn. Subsequently, this will reduce the Zr^{4+} content. For this purpose, additional molar ratios, 3:3:4 and 3:6:1, were synthesised to sparsely investigate the share of Zn^{2+} over Zr^{4+} for the remaining 70% content of the catalyst. The additional samples are labelled as CZZr-334 and CZZr-361 respectively.

2.3. Catalyst characterization

The generated precursors were analysed using the Scanning Electron Microscope (SEM), Brunauer-Emmett-Teller (BET), Temperature-Programmed Desorption (TPD), Temperature-Programmed Reduction (TPR), Thermal Gravimetric Analysis (TGA), X-ray Diffraction (XRD), Differential Scanning Calorimetry (DSC) and Differential Thermal Analysis (DTA).

The surface composition and structure of the catalysts were studied with a SEM. The porosity and surface area of the catalysts were obtained using BET method determined via N_2 adsorption/desorption isotherms at 77 K, using a Micrometrics ASAP 2020 Surface Area and Porosity Analyser. Here, 0.2–0.4 g of the samples was degassed under vacuum at 363 K for ~4 h before being dosed with N_2. The BET surface area was computed within the relative pressure range of 0.06–0.3 and the pore volume at a pre-determined relative pressure of 0.9948.

The TGA, DSC and DTA were performed using a NETZSCH STA-449-F3 Jupiter Thermal Analyser. 5–10 mg of the catalyst were weighed into the sample pan and was subjected to a decomposition temperature from 293 to 1073 K at a constant ramp of 10 and 20 K/min respectively under N_2.

XRD patterns were studied using a Bruker-AXS D8 advance powder diffractometer using Cu radiation with a scanning range of $10^\circ \leq 2\theta \leq 90^\circ$ at a step size of 0.010216°. Average crystallite size was estimated using the Scherrer's formula:

Equation 1: Scherrer's Formula

$$d = \frac{0.9\lambda}{\beta\cos\theta}$$

where d is the crystallite size (nm), λ is the radiation wavelength (nm) = 1.5406 nm in this case, β is the full width at half maximum (radians) and θ is the Bragg's angle of the maximum intense peak (degrees) [37].

CO_2-TPD was conducted using AutoChem II 2920 to assess the basicity of the catalysts. First, the 50 mg of the catalyst was reduced at 573 K for 1 h in a flow of H_2 at 30 ml/min. Subsequently, the catalyst was cooled to 323 K before being flushed with He for 0.5 h at same temperature at 40 ml/min. The catalyst was then exposed to pure CO_2 for 1 h at a flow rate of 30 ml/min before being flushed with He at 40 ml/min to remove all physisorbed molecules. TPD measurement was conducted at temperature range of 323–1073 K with a heating rate of 10 K/min under the flow of He at 40 ml/min, and the CO_2 desorption monitored using a thermal conductivity detector (TCD).

H_2-TPD experiment was performed in the same equipment as CO_2-TPD. 50 mg of the catalyst was first reduced in situ at 573 K for 2 h in mixed flow of H_2/He (10:90 vol%). After which, the catalyst was cooled down to 323 K and then saturated in 10% H_2/He for 1 h, followed by purging with N_2 for 0.5 h to remove any physisorbed molecules. H_2-TPD measurement was then performed to 1073 K with a heating rate of 5 K/min under N_2 atmosphere.

H_2 temperature program reduction (H_2-TPR) of catalysts (50 mg) was carried out in a U-tube quartz reactor using a Micromeritics ChemiSorb 2920 with a thermal conductivity detector (TCD). Before reduction, the sample was first degassed with He flow of 40 mL min^{-1} at 473 K for 60 min to remove physically adsorbed water and cooled down to the 333 K. Then the sample was reduced at a heating rate of 10 K min^{-1}–1023 K with 50 mL min^{-1} of 5% H2/Ar mixture gas.

2.4. Catalyst performance evaluation

The performance of the catalysts towards methanol synthesis was assessed in a continuous flow fixed bed reactor. First, 0.5 g of the catalyst was reduced at 623 K in H_2/N_2 (10/90 vol%) environment for 3 h at atmospheric pressure before being cooled to room temperature. The reactant gas H_2/CO_2 (molar ratio = 3:1) under operating conditions of 3 MPa, 623 K and gas hourly space velocity (GHSV) of 3100 h^{-1}. The effluent was analysed online using an Agilent gas chromatograph (GC) 7890A with the transfer line from the reactor to the GC preheated at 373 K to avoid condensation of effluent products. TCD was used to measure N_2, CO and CO_2 gases while organic compounds were studied using the flame ionization detector (FID). From this test, catalytic conversion and selectivity were computed using mass balance and resulting steady-state values (SSV). SSV was computed as an average of three tests over a period of 3 h of continuous operation. CO_2 conversion (x_{CO2}), selectivity (s_i) and yield (y_i) (where i is the molecule of interest) were computed as follows:

Equation 2: CO_2 conversion computation

$$X_{CO_2} = \frac{n_{CH_3OH} + n_{CO}}{n^0_{CO_2}}$$

Equation 3: Methanol and carbon monoxide selectivity computation

$$S_{CH_3OH} = \frac{n_{CH_3OH}}{n_{CH_3OH} + n_{CO}}$$

$$S_{CO} = \frac{n_{CO}}{n_{CH_3OH} + n_{CO}}$$

Equation 4: Computation of yield for methanol

$$Y_{CH_3OH} = s_{CH_3OH} \times x_{CO_2}$$

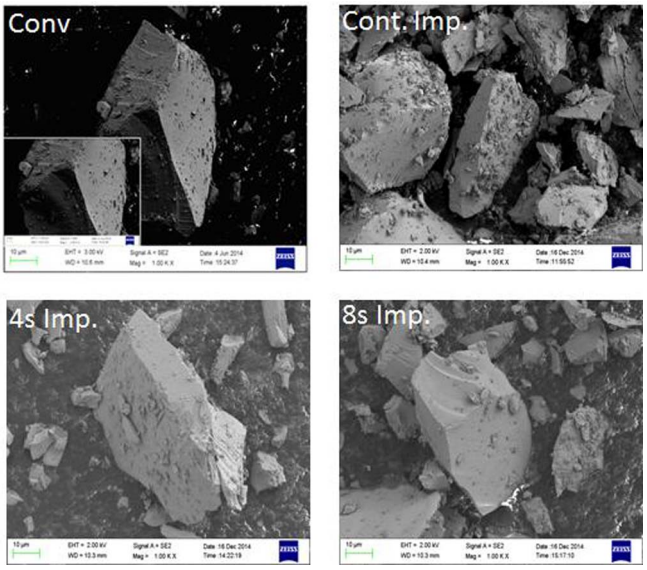

Fig. 1. SEM Analysis of CZr prepared via Ultrasonic Modulation at different Impulse times (continuous impulse (Cont. Imp.), 4 s and 8 s) in comparison with conventional co-precipitation method (Conv).

3. Results and discussions

3.1. Variation of surface morphology on ultrasonic modulation and metal composition

The Cu/ZrO_2 catalysts prepared via normal co-precipitation and ultrasonic-assisted co-precipitation method are shown in Fig. 1. SEM micrograph shows that the samples are of irregular shape with particle agglomeration. However, this is affected by the introduction of ultrasonic irradiation. Despite the similarity in particle boulder shape, agglomeration was observed to increase with decrease in impulse of ultrasonic irradiation. With no impulse (continuous impulse), agglomeration was attained its highest and least with 8 s impulse, which was slightly similar to the conventional catalyst. This stresses the impact of ultrasonic irradiation on the morphology, and probably, on the physical properties of the material [38]. Fig. 2 shows the surface morphology of the calcined CZZr catalysts. In each sample, possible cavities were observed all over the surface of the catalyst. This is attributed to the decomposition of formed citrates with an obvious caking of the particles [10]. The cavities and compactness or caking of the catalyst was detected to increase with increase in Cu/Zn ratio. This is similar to findings reported by Huang, Chen, Fei, Liu and Zhang [10].

The sorption isotherm obtained from the BET analysis for samples prepared with varying impulse time of ultrasonic irradiation was used to compute the surface area (S_{BET}), pore volume (V_P), and particle size (D_P). The results are tabulated in Table 1. The data indicates that an increase in surface area was obtained with decrease in impulse time. However, the particle size showed an appreciable decrease with decrease in pulse modulation. Moreover, there was an insignificant variation in V_p from 0.15 cm^3/g for the conventional CZr to 0.17 cm^3/g of the continuous-impulsed CZr. This can be attributed to the enhanced interaction as a result of continuous ultrasonic irradiation. This depicts an improvement in the pore structure of the samples and is attributed to the enhancement of nucleation and precipitate growth resulting from improved dissolution and reaction process via sonication [39,40]. When compared to the conventional samples (designated by conv), it was observed that at impulses greater than 1 s, sonication tends to have an adverse effect on the particle surface area. Nonetheless, with the introduction of Zn^{2+} metal ion into the composite oxide, the surface area and pore volume increased but varied inversely with increase in Cu^{2+}/Zn^{2+} ratio (Table 2). Although, not much difference was observed with pore volume. However, the particle diameter was detected to increase with Cu^{2+}/Zn^{2+} ratio. This can be associated with the additional interactions facilitated by the presence of the promoting metal ion. The observed trend corresponds with reported phenomenon and was explained that the variation in Cu/Zn ratio affects the crystal growth and particle agglomeration of the catalyst. This in turn alters the textural properties of the catalyst [10].

Table 1
BET results of CZr catalysts prepared at different ultrasonic impulse time.

Structural Characteristics	8 s Imp	4 s Imp	1 s Imp	Cont imp	Conv
BET Surface Area (m^2/g)	53.84	54.31	58.33	64.36	57.03
Pore Volume (cm^3/g)	0.15	0.14	0.14	0.17	0.15
Pore size (nm)	2.70	2.63	2.46	2.60	2.62
Average Particle Size (nm)	27.86	26.49	25.72	23.31	26.30

XRD pattern of the prepared samples are shown in Fig. 3. Fig. 3a shows the pattern for CZr catalysts at different ultrasonic modulation at constant Cu-loading of 30%. The pattern shows no difference in peak position. However, peak intensity was perceived to increase with ultrasonic irradiation at continuous impulse. This suggests that ultrasonic irradiation has limited impact in improving the crystallinity of the catalyst. The notable peaks observed were the tetragonal ZrO_2 (t-ZrO_2) at peak angles $2\theta = 62^\circ$, monoclinic ZrO_2 (m-ZrO_2) with peak angles $2\theta = 23^\circ$ and 28.2° and Cu species with peak angles $2\theta = 35.6^\circ$ related to CuO and $2\theta = 42.8^\circ$ and 72° related to Cu metal. Incorporating the metal Zn^{2+} to the CZr composite oxide, a series of overlapping peaks were obtained. The presence of CuO was indicated with peaks at $2\theta = 32.4^\circ$, 35.4° and 38.7°. The 35.4° peak overlapped with 36.3° peak for ZnO. Other ZnO peaks are at $2\theta = 31.8^\circ$ and 34.5°. Noticeably, as the Cu/Zn ratio decreases, the ZnO diffraction peaks increases as well relative to their individual CuO peak intensities. The diffraction peaks of ZrO_2 was also detected but as monoclinic at $2\theta = 23^\circ$ and 28.8° and as tetragonal at $2\theta = 30.3^\circ$. It is observed that the m-ZrO_2 which was the more dominant ZrO_2 crystal increased in accordance with its normal composition in the composite oxide. The crystallite size of CuO

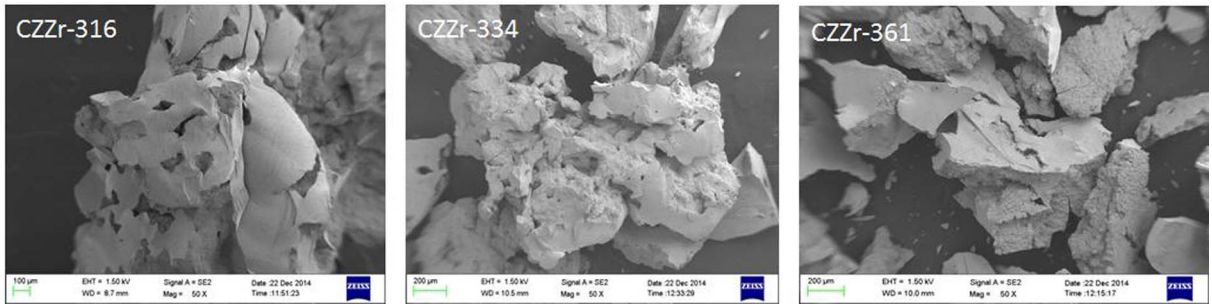

Fig. 2. SEM images of prepared CZZr catalysts at varying compositions and continuous impulse ultrasonic irradiation (CZZr-xyz indicates catalyst with Cu^{2+}:Zn^{2+}:Zr^{4+} molar ratio = x:y:z).

Table 2
BET and metallic composition analysis of CZZr catalysts prepared at different metallic composition.

Sample	Metallic Composition (wt%)[a]			Cu^{2+}:Zn^{2+}	S_{BET} (m^2/g)	V_P (cm^3/g)	D_P (nm)
	Cu^{2+}	Zn^{2+}	Zr^{4+}				
CZZr-316	30.52	15.36	54.12	3.0	64.71	0.17	23.31
CZZr-334	32.19	31.37	36.44	1.0	68.52	0.20	21.36
CZZr-361	31.45	60.82	7.73	0.5	70.38	0.21	15.82

[a] Computed by atomic emission spectroscopy (AES).

crystal was computed using the Scherrer's equation as 16.64, 19.99 and 19.63 nm for CZZr-316, CZZr-334 and CZZr-361 respectively. This indicates that the presence of Zn^{2+} has an impact on the crystallinity and relative dispersion of Cu. Crystallinity of the catalyst is suggested to be highest at moderate composition of Zn^{2+}.

3.2. Thermal characteristics

The thermal strength of the prepared catalysts with varying ultrasonic modulation is shown in Fig. 4. It is detected that there are three decomposition steps in all cases. Although this varied with the level of ultrasonic impulse. As shown in the figure, the first decomposition step (of both weight loss and DTA plot) occurred at temperature less than 250 °C. This is associated with the loss of moisture and is identified by the lowest peak of the DTA plot. The second decomposition step as a result of interstitial moisture loss is existed between 250 and maximum temperature of *ca.* 680 °C. Maximum temperature of the second decomposition peak varied with impulse of ultrasonic irradiation with continuous and 1 s impulse having the highest. Beyond this temperature is the loss of NO_3^- attached to the surface of the catalyst. This explains that the thermal stability of the catalyst was enhanced by ultrasonic modulation. Nonetheless, this is dependent on the intensity of the irradiation. With a continuous or near-continuous impulse, a more thermal stable material is obtained. In terms of energy required for the thermal breakdown of the catalyst, Fig. 5 was obtained. This is the DSC analysis of the prepared catalysts within a temperature range of 0–800 °C. The result validates the thermal stability of samples prepared at continuous and 1 s impulse. This is observed from to the plot to be closest to the zero DSC line indicating a minimal energy differential per

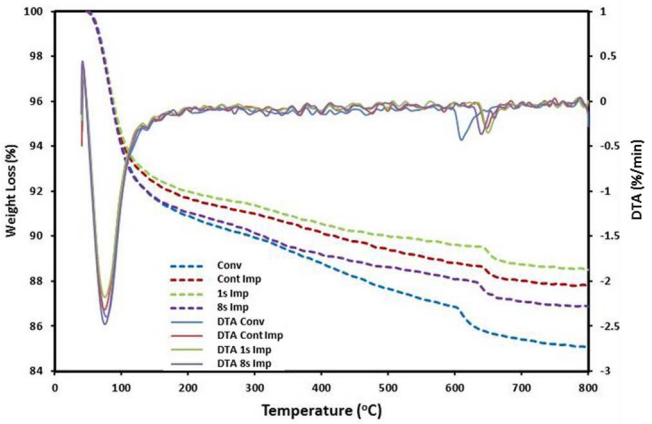

Fig. 4. TGA-DTA profile for CZr catalysts.

mass of the sample. In the profile, it is also noteworthy that the loss of NO_3^- was at a more extended temperature than that of the conventional and higher impulse samples.

Varying the heating rate, it is shown that a better thermal stability is achieved at 20 K/min as shown in Fig. 6. The 20 K/min profile for both continuous and 1 s impulse were observed to be have the minimal change in energy (closest to the zero line). In addition, it is also witnessed that at 20 K/min, the breakdown peaks of the catalysts (solid lines) occurred at higher temperatures than that of 10 K/min (broken lines). This suggests that for optimum industrial applicability, the material will be well suited at a thermal operation with heating rate at

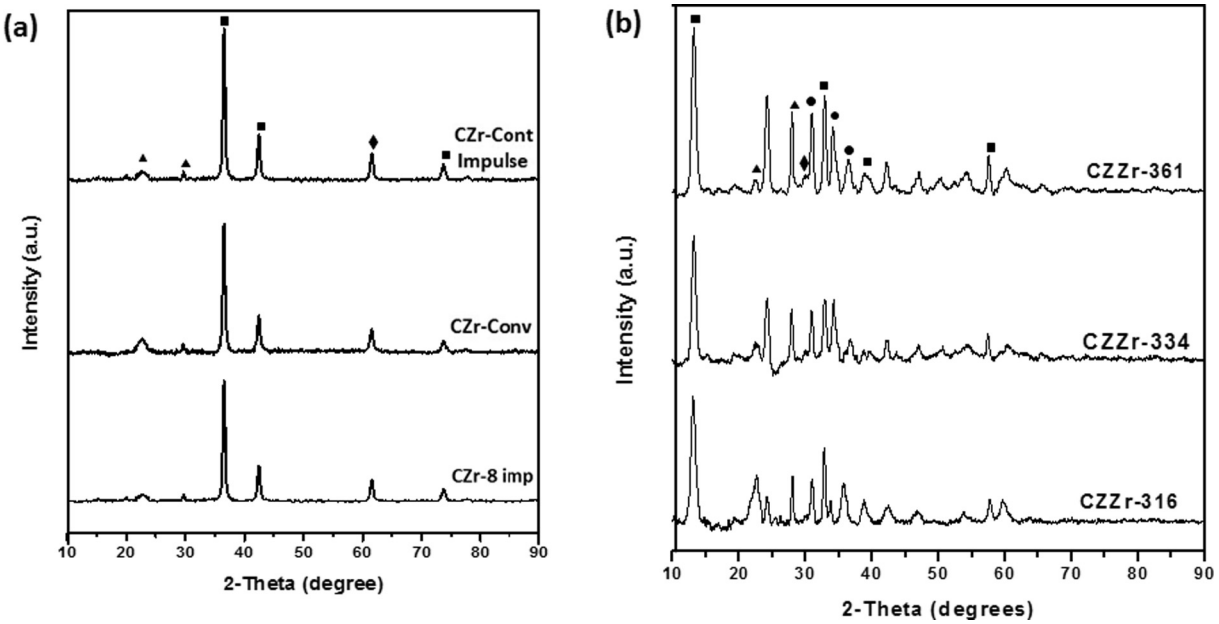

Fig. 3. XRD pattern for (a) calcined CZr catalysts prepared with variation in ultrasonic impulse at Cu-loading of 30 wt%, and (b) CZZr catalyst prepared with difference in metallic composition. (□) CuO, (○) ZnO, (◊) t-ZrO_2 and (Δ) m- ZrO_2.

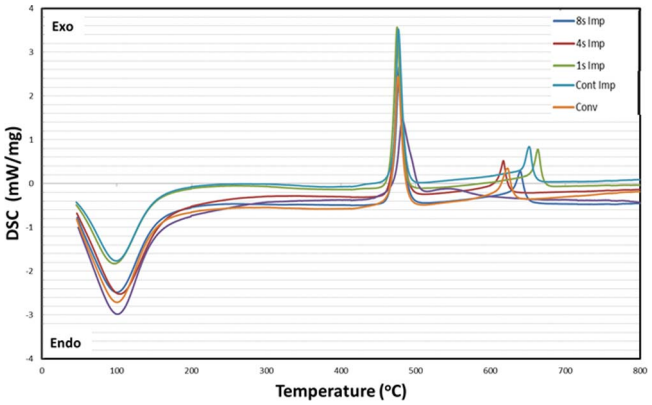

Fig. 5. DSC profile for CZr catalysts at different ultrasonic impulse.

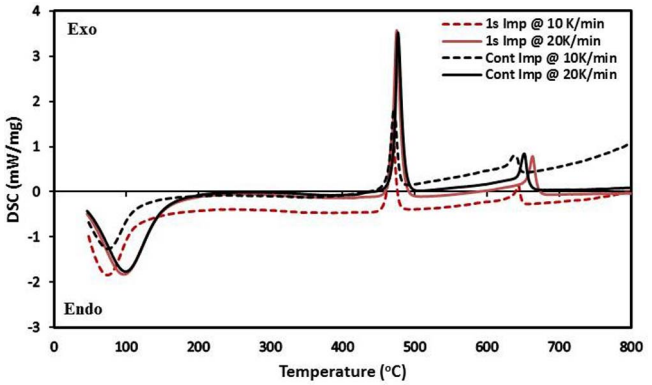

Fig. 6. DSC analysis at different heating rate for CZr catalysts prepared with ultrasonic irradiation at 1 s and continuous impulse.

20 K/min rather than 10 K/min. Since the thermal stability of this catalyst is directly proportional to Zr^{4+} content [3,4], the thermal characteristics of CZZr was neglected.

3.3. Reducibility of catalysts

To understand the reducibility of the catalysts, H_2-TPR analysis was conducted. The results are as shown in Fig. 7. Three classes of adsorption peaks were observed for the catalysts depending on the preparation method and composition of metal. In accordance with literature, the first peak (α) occurred at low temperature range (100–300 °C) and is attributed to the adsorption of atomic hydrogen highly dispersed Cu^{2+}. The second desorption peak (β) occurred at mid temperature range from 300 to 500 °C, assigned to the adsorption of hydrogen on moderately dispersed Cu^{2+} species. The final peak (γ) situated at temperature range 500–700 °C is associated with hydrogen adsorption by bulk Cu^{2+} species [41–44]. Fig. 7a shows the profile for CZr reduction. Reducing the radiation impulse resulted to an increase in the intensity of α-peak and decrease in β-peak. High temperature adsorption of H_2 was not witnessed in this catalysts. This suggests that the increase in ultrasonic impact (designated by reduced impulse time) will aid in high Cu dispersion. The quantitative analysis of this effect is summarised in Table 3. Fig. 7b shows the profile for CZZr at varying amount of Zn^{2+} ion. At low amount of zinc (CZZr-316), the α-peak was still detected alongside with the detection of a β'-peak, which can be explained to be due to difficulties in the reduction of some dispersed Cu [43]. However, both peaks tend to fade as the composition of Zn increased. This is associated with an increase in intensity, reduction in width and shift of β-peak towards a higher temperature. A logical explanation can be given that the presence of Zn increases the dispersion of Cu species and makes it more accessible for potential dissociation of hydrogen molecule [10]. In this set of catalysts, the γ-peaks were observed and this tends to increase with increase in the amount of Zn. These results show that the amount of easily reducible well dispersed and bulk CuO increased with increase in Zn (Table 3). The result data also shows that the impact of introduction of Zn promoter outweighs

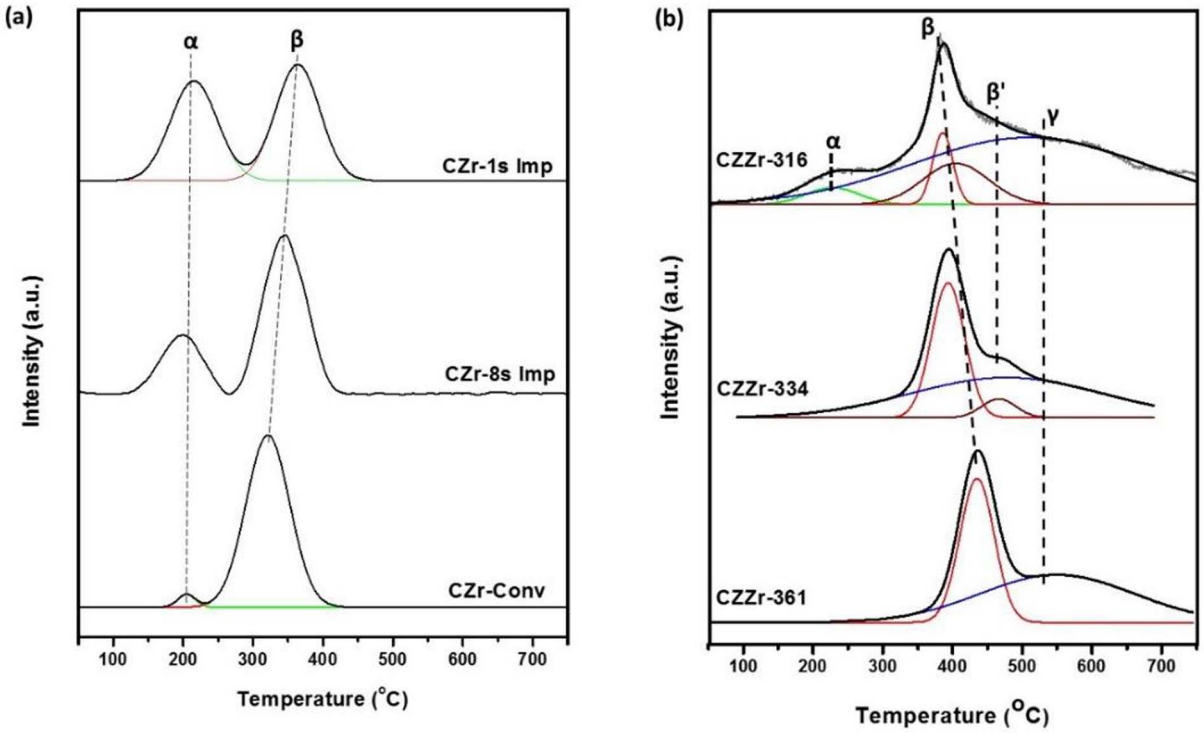

Fig. 7. TPR profile of (a) CZr catalyst at various ultrasonic impulse, and (b) CZZr Catalyst at different metal composition.

Table 3
Peak areas of H_2-TPD profiles of reduced CZr and CZZr catalysts.

Sample	Peak Areas (a.u.)				Total Area (a.u.)
	α-peak	β-peak	β′-peak	γ-peak	
CZr-1s Impulse	2.74	3.04	–	–	5.78
CZr-8s Impulse	0.13	4.42	–	–	4.55
CZr-Conv	0.03	4.52	–	–	4.55
CZZr-316	3.32	11.61	15.89	1.84	32.66
CZZr-334	–	22.67	3.27	39.03	64.97
CZZr-361	–	28.98	–	42.39	71.37

the impact of ultrasonic modulation. For instance, comparing the total peak area of CZr at 1 s impulse and CZZr-316 with that of the conventional catalyst, it is estimated that the difference between the former is a unit magnitude while the latter is of 6-fold magnitude difference.

3.4. H_2 desorption

The H_2-TPD pattern for the pre-reduced catalysts was also studied (see [8]). The desorption profile spanned across a temperature range 50–800 °C and displayed several adsorption states of H-species on the catalysts. These peaks are classed into two categories, low (130–300 °C) and high (400–500 °C) temperature peaks designated as α and β peaks respectively [16,43,45]. Desorption at low and high temperature region is ascribed to the release of H-species adsorbed on surface Cu sites and on surface ZnO or ZrO_2 respectively. Fig. 8a shows that as the impulse time reduces, the intensity of the peaks increased indicating that an increased impact in ultrasonic irradiation will boost the amount of surface Cu sites and available metal oxides. Hydrogen spillover phenomenon is suggested to facilitate the hydrogen adsorption process on ZnO and ZrO_2 sites [16,45]. For the CZZr catalysts, two peaks were equally obtained within the reported temperature range. However, it was observed that both peaks had broader bands that the CZr catalysts. This is attributed to the presence of the Zn promoter which aids in increasing the amount of Cu active sites. CZZr-316 with the lowest composition of Zn showed the basic α and β peaks. But with an increase in Zn composition resulted to an increase in peak intensity with the detection of additional peaks, α′ and β′ peaks as shown in Fig. 8b. The α′-peak can be attributed to both physical and chemical interactions between Cu and the metal oxides with an alteration in electron distribution, which will facilitate the adsorption of hydrogen [42]. The β′ peak can be explained as a separated hydrogen adsorption on the individual ZnO and ZrO_2 surface sites. With further increase in Zn composition (CZZr-361), the intensity of the peaks was reduced. It may be suggested that above a specific metal composition, hydrogen adsorption will be deterred by the metals. Li, Mao, Yu and Guo [9] suggested that this interaction could be facilitated by the sintering effect [9], which in turn will result to reduction in surface area [10]. In conclusion, the best catalyst for the purpose of methanol synthesis via hydrogenation process is one with a better H_2 adsorption strength and good desorption of the dissociated hydrogen atom [46]. Emphasis for the selection of these catalysts should be based on the α-peak desorption profile because it is the hydrogen desorbed from this peak region that will be made available for the hydrogenation process [47].

3.5. Surface basicity of catalysts

The surface basicity of the catalysts were studied using the CO_2-TPD technique. The desorption profiles and data are shown in Fig. 9 and Table 4 respectively. Generally, the basicity of metal oxides are categorized into three: weak, medium (or moderate) and strong basic strengths. In this study, these three zones are depicted at their corresponding temperature peaks ranging from 100to 160 °C, 300 to 550 °C and > 600 °C respectively. Weak basic sites (α) are associated with the surface hydroxyl (OH^-) group; whereas the moderate basic sites (β) are related to metal–oxygen (M^{n+}-O^{2-}, where n+ is the valence of the metal) pair. The strong basic sites (γ) are attributed to the low coordination unsaturated oxygen (O^{2-}) and electronegative anions [43]. Fig. 9a shows TPD profile for CZr catalysts at varying modulation impulse. As can be seen, peak intensities increased with increase in impact

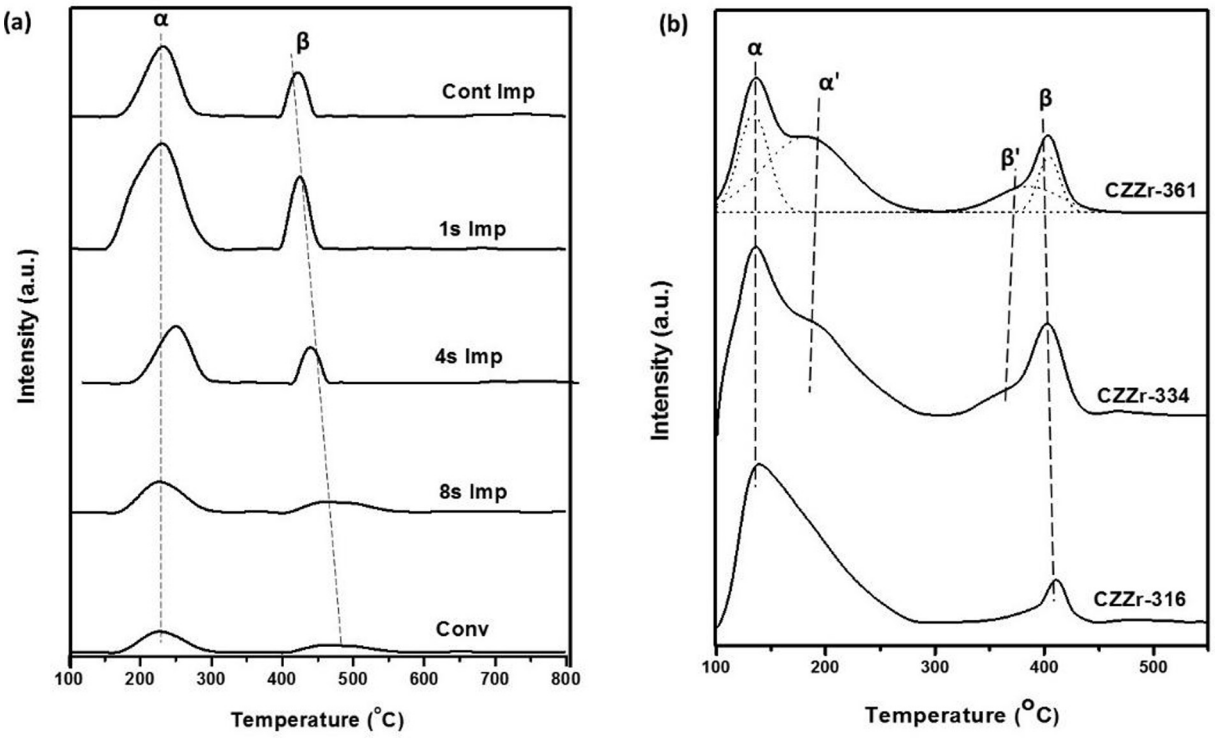

Fig. 8. H_2-TPD profile for (a) reduced CZr at various ultrasonic impulse time, and (b) CZZr catalysts at different metal composition.

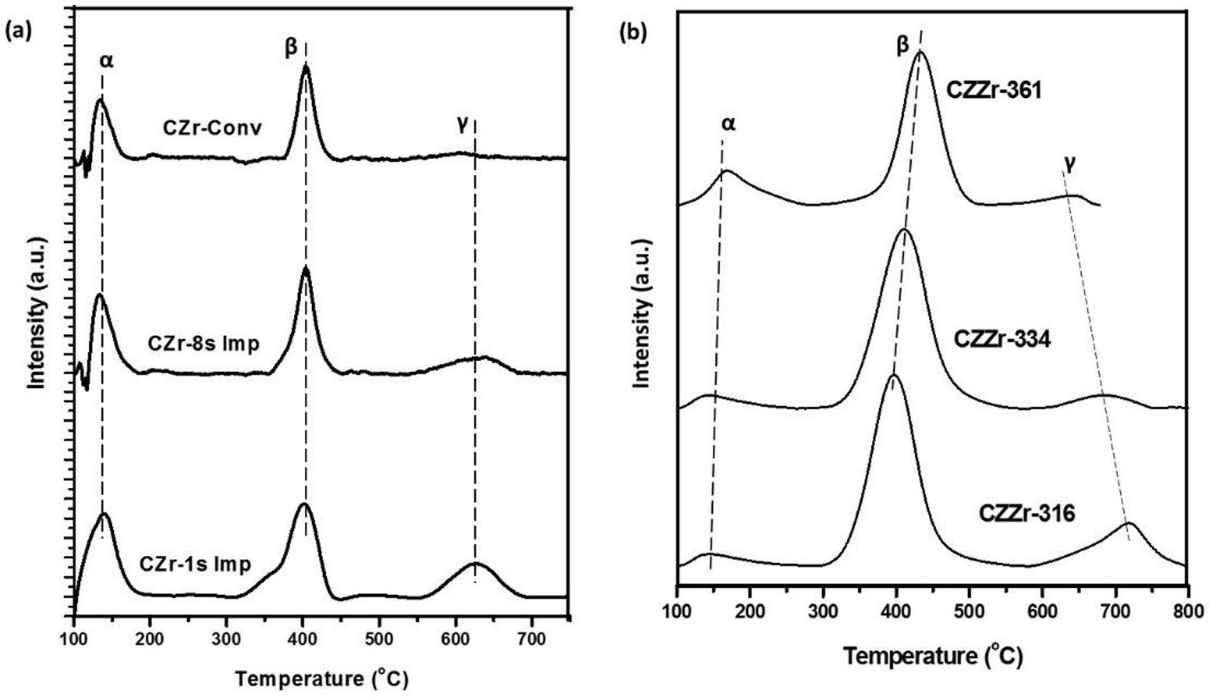

Fig. 9. CO_2 desorption profile for (a) reduced CZr at various ultrasonic impulse time, and (b) CZZr catalysts at different metal composition.

Table 4
Result data for CO_2 desorption profile for reduced CZr and CZZr catalysts.

Sample	Weak Basic Site		Medium Basic Sites		Strong Basic Sites		Total (a.u.)
	Temp. (°C)	Peak Area (a.u.)	Temp. (°C)	Peak Area (a.u.)	Temp. (°C)	Peak Area (a.u.)	
CZr-Conv	148.00	3.53	400.00	8.67	620.00	0.06	12.26
CZr-8s Imp	147.00	4.31	399.00	9.31	632.00	1.35	14.97
CZr-4s Imp	147.00	4.99	400.00	8.48	630.00	2.49	15.96
CZr-1s Imp	148.00	5.84	400.00	11.43	625.00	5.43	22.70
CZr-Cont Imp	147.00	5.46	401.00	10.91	630.00	5.52	21.89
CZZr-361	148.00	6.53	412.00	30.23	658.00	0.86	37.62
CZZr-334	148.00	6.18	409.00	33.86	699.00	2.14	42.18
CZZr-316	160.00	5.30	400.00	39.71	717.00	10.82	55.83

Table 5
Catalytic performance of CZr and CZZr catalysts for methanol synthesis.[‡]

Sample	X_{CO2} (%)	S_{CH3OH} (%)	S_{CO} (%)	Y_{CH3OH} (%)
Variation with ultrasonic impulse				
CZr-Conv	5.71	48.92	51.08	2.79
CZr-Cont Imp	8.43	50.31	49.69	4.24
CZr-1s Imp	8.82	50.72	49.28	4.47
CZr-4s Imp	6.36	49.16	50.84	3.13
CZr-8s Imp	5.67	47.83	52.17	2.71
Variation with metal composition				
CZZr-316	17.78	54.28	48.72	9.65
CZZr-334	18.68	53.57	46.43	10.01
CZZr-361	17.08	49.93	49.07	8.53

[‡] Reaction conditions: P = 3.0 MPa, T = 623 K, GHSV = 3100 h^{-1}, CO_2:H_2 = 1:3. Experimental errors = ± 4.6%.

of ultrasonic modulation. Hence, ultrasonic irradiation has yet proven to improve the surface basicity of the catalyst. This can be attributed to the enhanced surface morphology of the catalyst hence making the basic sites accessible for CO_2 adsorption. Fig. 9b portrays the CO_2 desorption profile for the CZZr catalysts prepared at different metal composition. Result data shows that a variation of metal composition has an impact on the surface basicity of the catalyst. As Cu/Zn ratio (also associated with the increase in Zr^{2+} content) increases, the intensity of α-peaks decreased but the β and γ-peaks showed an appreciable increase in intensity. The increase in moderate and strong basic sites can be attributed to the increase in Zr^{4+} content since this metal is suggested to have a great synergetic effect on CO_2 desorption at moderate and strong basic sites when compared to Zn^{2+} [10]. Additionally, the γ-peak was observed to shift towards higher temperature with increase in Cu/Zn ratio. This is suggested to be due to the increased electron density of the strong basic sites, and can be attributed to the aggregation of saturated O^{2-} ions [43].

3.6. Catalytic performance for methanol synthesis

In this study, the catalytic performance was evaluated based on the catalytic selectivity and activity for CO_2 hydrogenation. The results are shown in Table 5. From the obtained results, it is observed that CO_2 conversion increased with increased impact of sonication. As the sonication impulse reduced from 8 s to 1 s, CO_2 conversion increased from 5.67% to 8.82%. This can be explained using the H_2-TPD data within the neighbourhood of the reaction temperature. The principle of H_2-TPD discloses the ease of hydrogen adsorption on Cu-sites. This is assumed to reflect the reducibility of the catalyst, hence showing readily

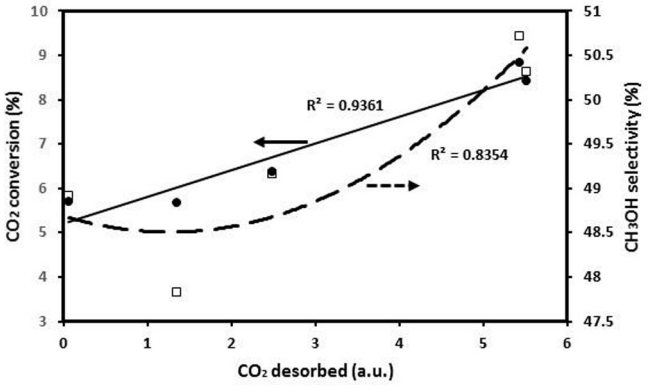

Fig. 10. Correlation between CO_2-TPD data with CO_2 conversion and CH_3OH selectivity for CZr catalyst.

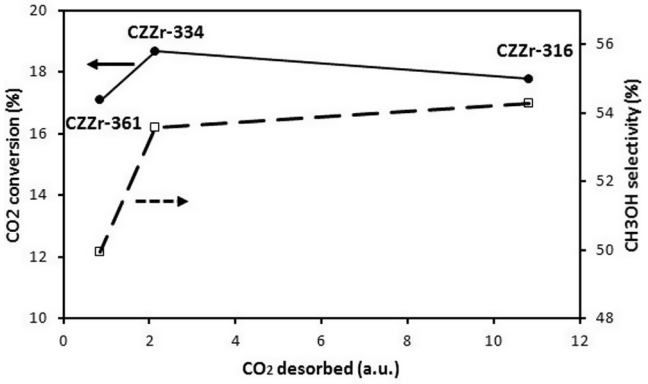

Fig. 11. Correlation between CO_2-TPD data with CO_2 conversion and CH_3OH selectivity for CZZr catalyst.

available active Cu-sites for hydrogen dissociation. This will facilitate CO_2 conversion. Hence, the high CO_2 conversion capacity of this catalyst can be related tentatively to its high adsorption of hydrogen within the reaction temperature of 623 K (350 °C). Furthermore, it was observed that methanol selectivity was highest with the 1 s impulse sample (50.72%) and least in CZr-8s impulse sample (47.83%). This can be attributed to various factors [48,49]. Recent studies proposed that the surface basicity of the catalyst plays a key role in the catalytic selectivity. It is promulgated that CO_2 adsorbed at the strong basic sites favourably promotes methanol synthesis over RWGS [43,45,50]. The adsorbed CO_2 at this sites will hardly be reduced to CO. The results from CO_2-TPD shows that both intensity and contribution of strong basic sites is highest with the 1 s impulse sample and least in the conventional CZr catalyst. With these parameters, the methanol yield was estimated with samples with frequent ultrasonic irradiation having the highest yields. Correlating the amount of CO_2 desorbed to the CO_2 conversion and methanol yield, a linear relationship was obtained for the former. This suggests that the amount of CO_2 converted is directly related to the amount adsorbed. Whereas, for methanol selectivity, a minimum is attained before it begins to ascend. This is as a result of the simultaneous occurrence of reverse water gas shift reaction with the production of CO (see Fig. 10).

The presence of Zn in the catalyst is also considered to affect the conversion of CO_2 and selectivity of methanol. As the Cu/Zn ratio decreases from 3 to 0.5, the conversion of CO_2 showed an initial increase from 17.78% to 18.68% before descending to 17.08%. This corresponds to the H_2-TPD profile of these catalysts validating the effect of dissociative desorption of hydrogen on hydrogenation of CO_2. Moreover, the increase in Cu/Zn ratio was associated with an increase in methanol selectivity. This is at par with the CO_2-TPD results for strong basic sites. Correlating the CO_2 desorption profile at this basic sites with the methanol selectivity and CO_2 conversion, it can be proposed that at a low Cu/Zn ratio (< 1), the methanol selectivity and CO_2 conversion displays a sharp reduction slope. But at higher Cu/Zn ratio (> 1), a low change gradient is observed for both selectivity and conversion of methanol and CO_2 respectively. This is diagrammatically illustrated in Fig. 11.

4. Conclusions

In the synthesis of methanol via hydrogenation process, one key contributor to the effectiveness of this process is the presence of a suitable catalyst. The most suitable and widely used catalyst is the Cu-based catalyst and its optimal performance is based partly on its thermal characteristics and surface morphology and chemistry. Subsequently, this is dependent on various factors including catalyst synthetic method, metal content and composition. In addition, its thermal strength is also dependent on the heating rate. The effect of these factors are summarised as follows based on the results of the current study:

1. The adoption of ultrasonic irradiation at different sonication impulse affects particle agglomeration, which in turn contributes to the surface morphology and chemistry of the Cu/ZrO_2 catalysts. Low sonication impulses displayed the best properties for the catalyst with improved surface area, particle size and porosity.
2. Metal promoter, ZnO had a greater impact on these properties with an optimum performance at moderate Zn content.
3. Based on the thermal tests, this study suggests that for optimum industrial applicability, the material will be well suited at a thermal operation with heating rate at 20 K/min rather than 10 K/min.

Acknowledgments

This work was carried out at the International Doctoral Innovation Centre (IDIC). The authors would like to acknowledge the financial support through the grant of Ningbo Key Research Project ‘Absorption/catalytic technologies for the simultaneous removal of multi-pollutants from flue gas at power stations’ (Grant No. 1012B10042) and from Ningbo Education Bureau, Ningbo Science and Technology Bureau, China's MoST and The University of Nottingham. The work is also partially supported by EPSRC (Grant No. EP/G037345/1) and Ningbo Innovation Team Project on ‘Indoor air pollution control technology’ (Grant No. 2017C510001).

References

[1] K. Fujimoto, Y. Yu, Spillover effect on the stabilization of Cu-Zn catalyst for CO_2 hydrogenation to methanol, Stud. Surf. Sci. Catal. 77 (1993) 393–396.
[2] F. Arena, K. Barbera, G. Italiano, G. Bonura, L. Spadaro, F. Frusteri, Synthesis, characterization and activity pattern of Cu–ZnO/ZrO_2 catalysts in the hydrogenation of carbon dioxide to methanol, J. Catal. 249 (2007) 185–194.
[3] C. Li, X. Yuan, K. Fujimoto, Development of highly stable catalyst for methanol synthesis from carbon dioxide, Appl. Catal. A 469 (2014) 306–311.
[4] S. Natesakhawat, J.W. Lekse, J.P. Baltrus, P.R. Ohodnicki, B.H. Howard, X. Deng, C. Matranga, Active sites and structure-activity relationships of copper-based catalysts for carbon dioxide hydrogenation to methanol, ACS Catal. 2 (2012) 1667–1676.
[5] J. Słoczyński, R. Grabowski, A. Kozłowska, P. Olszewski, M. Lachowska, J. Skrzypek, J. Stoch, Effect of Mg and Mn oxide additions on structural and adsorptive properties of Cu/ZnO/ZrO_2 catalysts for the methanol synthesis from CO_2, Appl. Catal. A 249 (2003) 129–138.
[6] J. Słoczyński, R. Grabowski, A. Kozłowska, M. Lachowska, J. Skrzypek, Effect of additives and a preparation method on catalytic activity of Cu/ZnO/ZrO_2 system in the carbon dioxide hydrogenation to methanol, Stud. Surf. Sci. Catal. 153 (2004) 161–164.
[7] J. Słoczyński, R. Grabowski, P. Olszewski, A. Kozłowska, J. Stoch, M. Lachowska, J. Skrzypek, Effect of metal oxide additives on the activity and stability of Cu/ZnO/ZrO_2 catalysts in the synthesis of methanol from CO_2 and H_2, Appl. Catal. A 310 (2006) 127–137.
[8] M. Lachowska, J. Skrzypek, Methanol synthesis from carbon dioxide and hydrogen over Mn-promoted copper/zinc/zirconia catalysts, React. Kinet. Catal. Lett. 83

(2004) 269–273.
[9] L. Li, D. Mao, J. Yu, X. Guo, Highly selective hydrogenation of CO_2 to methanol over CuO–ZnO–ZrO_2 catalysts prepared by a surfactant-assisted co-precipitation method, J. Power Sources 279 (2015) 394–404.
[10] C. Huang, S. Chen, X. Fei, D. Liu, Y. Zhang, Catalytic hydrogenation of CO_2 to methanol: study of synergistic effect on adsorption properties of CO_2 and H_2 in CuO/ZnO/ZrO_2 system, Catalysts 5 (2015) 1846.
[11] Y. Ma, Q. Sun, D. Wu, W.-H. Fan, Y.-L. Zhang, J.-F. Deng, A practical approach for the preparation of high activity Cu/ZnO/ZrO_2 catalyst for methanol synthesis from CO_2 hydrogenation, Appl. Catal. A 171 (1998) 45–55.
[12] R. Raudaskoski, M.V. Niemelä, R.L. Keiski, The effect of ageing time on co-precipitated Cu/ZnO/ZrO_2 catalysts used in methanol synthesis from CO_2 and H_2, Top. Catal. 45 (2007) 57–60.
[13] E. Frei, A. Schaadt, T. Ludwig, H. Hillebrecht, I. Krossing, The influence of the precipitation/ageing temperature on a Cu/ZnO/ZrO_2 catalyst for methanol synthesis from H_2 and CO_2, ChemCatChem 6 (2014) 1721–1730.
[14] M. Saito, T. Fujitani, M. Takeuchi, T. Watanabe, Development of copper/zinc oxide-based multicomponent catalysts for methanol synthesis from carbon dioxide and hydrogen, Appl. Catal. A 138 (1996) 311–318.
[15] J. Słoczyński, R. Grabowski, A. Kozłowska, P. Olszewski, J. Stoch, J. Skrzypek, M. Lachowska, Catalytic activity of the M/(3ZnO·ZrO_2) system (M = Cu, Ag, Au) in the hydrogenation of CO_2 to methanol, Appl. Catal. A 278 (2004) 11–23.
[16] F. Arena, G. Italiano, K. Barbera, S. Bordiga, G. Bonura, L. Spadaro, F. Frusteri, Solid-state interactions, adsorption sites and functionality of Cu-ZnO/ZrO_2 catalysts in the CO_2 hydrogenation to CH_3OH, Appl. Catal. A 350 (2008) 16–23.
[17] F. Arena, G. Italiano, K. Barbera, G. Bonura, L. Spadaro, F. Frusteri, Basic evidences for methanol-synthesis catalyst design, Catal. Today 143 (2009) 80–85.
[18] R. Raudaskoski, E. Turpeinen, R. Lenkkeri, E. Pongrácz, R.L. Keiski, Catalytic activation of CO_2: Use of secondary CO_2 for the production of synthesis gas and for methanol synthesis over copper-based zirconia-containing catalysts, Catal. Today 144 (2009) 318–323.
[19] F. Arena, G. Mezzatesta, G. Zafarana, G. Trunfio, F. Frusteri, L. Spadaro, Effects of oxide carriers on surface functionality and process performance of the Cu–ZnO system in the synthesis of methanol via CO_2 hydrogenation, J. Catal. 300 (2013) 141–151.
[20] R. Ladera, F.J. Pérez-Alonso, J.M. González-Carballo, M. Ojeda, S. Rojas, J.L.G. Fierro, Catalytic valorization of CO_2 via methanol synthesis with Ga-promoted Cu–ZnO–ZrO_2 catalysts, Appl. Catal. B 142 (2013) 241–248.
[21] X. Liu, P. Ramírez de la Piscina, J. Toyir, N. Homs, CO_2 reduction over Cu-ZnGaMO (M = Al, Zr) catalysts prepared by a sol-gel method: Unique performance for the RWGS reaction, Catalysis Today, doi: https://doi.org/10.1016/j.cattod.2017.04.022(2017).
[22] S. Esposito, M. Turco, G. Bagnasco, C. Cammarano, P. Pernice, New insight into the preparation of copper/zirconia catalysts by sol–gel method, Appl. Catal. A 403 (2011) 128–135.
[23] G. Bonura, M. Cordaro, C. Cannilla, F. Arena, F. Frusteri, The changing nature of the active site of Cu-Zn-Zr catalysts for the CO_2 hydrogenation reaction to methanol, Appl. Catal. B 152 (2014) 152–161.
[24] X. Guo, D. Mao, G. Lu, S. Wang, G. Wu, CO_2 hydrogenation to methanol over Cu/ZnO/ZrO_2 catalysts prepared via a route of solid-state reaction, Catal. Commun. 12 (2011) 1095–1098.
[25] X. Guo, D. Mao, G. Lu, S. Wang, G. Wu, Glycine–nitrate combustion synthesis of CuO–ZnO–ZrO_2 catalysts for methanol synthesis from CO_2 hydrogenation, J. Catal. 271 (2010) 178–185.
[26] X. Guo, D. Mao, S. Wang, G. Wu, G. Lu, Combustion synthesis of CuO–ZnO–ZrO_2 catalysts for the hydrogenation of carbon dioxide to methanol, Catal. Commun. 10 (2009) 1661–1664.
[27] F. Liao, Y. Huang, J. Ge, W. Zheng, K. Tedsree, P. Collier, X. Hong, S.C. Tsang, Morphology-dependent interactions of ZnO with Cu nanoparticles at the materials' interface in selective hydrogenation of CO_2 to CH_3OH, Angew. Chem. Int. Ed. 50 (2011) 2162–2165.
[28] M.-F. Luo, J.-M. Ma, J.-Q. Lu, Y.-P. Song, Y.-J. Wang, High-surface area CuO–CeO_2 catalysts prepared by a surfactant-templated method for low-temperature CO oxidation, J. Catal. 246 (2007) 52–59.
[29] L. Qi, Q. Yu, Y. Dai, C. Tang, L. Liu, H. Zhang, F. Gao, L. Dong, Y. Chen, Influence of cerium precursors on the structure and reducibility of mesoporous CuO-CeO_2 catalysts for CO oxidation, Appl. Catal. B 119 (2012) 308–320.
[30] Z. Wang, Z. Qu, X. Quan, Z. Li, H. Wang, R. Fan, Selective catalytic oxidation of ammonia to nitrogen over CuO-CeO_2 mixed oxides prepared by surfactant-templated method, Appl. Catal. B 134 (2013) 153–166.
[31] X. Ma, X. Feng, X. He, H. Guo, L. Lv, J. Guo, H. Cao, T. Zhou, Mesoporous CuO/CeO_2 bimetal oxides: One-pot synthesis, characterization and their application in catalytic destruction of 1,2-dichlorobenzene, Microporous Mesoporous Mater. 158 (2012) 214–218.
[32] C.I. Ezeh, X. Huang, X. Yang, C.-G. Sun, J. Wang, Sonochemical surface functionalization of exfoliated LDH: Effect on textural properties, CO_2 adsorption, cyclic regeneration capacities and subsequent gas uptake for simultaneous methanol synthesis, Ultrason. Sonochem. 39 (2017) 330–343.
[33] C.I. Ezeh, M. Tomatis, X. Yang, J. He, C. Sun, Ultrasonic and hydrothermal mediated synthesis routes for functionalized Mg-Al LDH: comparison study on surface morphology, basic site strength, cyclic sorption efficiency and effectiveness, Ultrason. Sonochem. 40 (2018) 341–352.
[34] R. Lewis Clark, Y. Wu, Electrohydrodynamic Processing of Micro- and Nanometer Biological Materials, Biomaterials Fabrication and Processing Handbook, CRC Press, 2008, pp. 275–333.
[35] S. Pradhan, J. Hedberg, E. Blomberg, S. Wold, I. Odnevall Wallinder, Effect of sonication on particle dispersion, administered dose and metal release of non-functionalized, non-inert metal nanoparticles, J. Nanopart. Res. 18 (2016) 285.
[36] A. Siddiqui, A. Alayoubi, Y. El-Malah, S. Nazzal, Modeling the effect of sonication parameters on size and dispersion temperature of solid lipid nanoparticles (SLNs) by response surface methodology (RSM), Pharm. Dev. Technol. 19 (2014) 342–346.
[37] A. Fathy, O. Elkady, A. Abu-Oqail, Synthesis and characterization of Cu–ZrO_2 nanocomposite produced by thermochemical process, J. Alloy. Compd. 719 (2017) 411–419.
[38] H. Xu, B.W. Zeiger, K.S. Suslick, Sonochemical synthesis of nanomaterials, Chem. Soc. Rev. 42 (2013) 2555–2567.
[39] C.I. Ezeh, M. Tomatis, X. Yang, J. He, C.-G. Sun, Ultrasonic and hydrothermal mediated synthesis routes for functionalized Mg-Al LDH: comparison study on surface morphology, basic site strength, cyclic sorption efficiency and effectiveness, Ultrason. Sonochem., doi:10.1016/j.ultsonch.2017.07.013.
[40] H.W. Olfs, L.O. Torres-Dorante, R. Eckelt, H. Kosslick, Comparison of different synthesis routes for Mg–Al layered double hydroxides (LDH): Characterization of the structural phases and anion exchange properties, Appl. Clay Sci. 43 (2009) 459–464.
[41] X. Dong, H.-B. Zhang, G.-D. Lin, Y.-Z. Yuan, K.R. Tsai, Highly active CNT-promoted Cu–ZnO–Al_2O_3 catalyst for methanol synthesis from H_2/CO/CO_2, Catal. Lett. 85 (2003) 237–246.
[42] J.A. Ahlers, J.A. Grasser, B.T. Loveless, D.S. Muggli, Room-temperature oxidation of reduced Cu/ZnO surfaces by lattice oxygen diffusion, Catal. Lett. 114 (2007) 185–191.
[43] P. Gao, H. Yang, L. Zhang, C. Zhang, L. Zhong, H. Wang, W. Wei, Y. Sun, Fluorinated Cu/Zn/Al/Zr hydrotalcites derived nanocatalysts for CO_2 hydrogenation to methanol, Journal of CO_2 Utilization, 16 (2016) 32–41.
[44] H. Wilmer, T. Genger, O. Hinrichsen, The interaction of hydrogen with alumina-supported copper catalysts: a temperature-programmed adsorption/temperature-programmed desorption/isotopic exchange reaction study, J. Catal. 215 (2003) 188–198.
[45] X. Guo, D. Mao, G. Lu, S. Wang, G. Wu, The influence of La doping on the catalytic behavior of Cu/ZrO_2 for methanol synthesis from CO_2 hydrogenation, J. Mol. Catal. A: Chem. 345 (2011) 60–68.
[46] L. Zhang, Y. Zhang, S. Chen, Effect of promoter SiO_2, TiO_2 or SiO_2-TiO_2 on the performance of CuO-ZnO-Al_2O_3 catalyst for methanol synthesis from CO_2 hydrogenation, Appl. Catal. A 415–416 (2012) 118–123.
[47] H. Zhan, F. Li, P. Gao, N. Zhao, F. Xiao, W. Wei, L. Zhong, Y. Sun, Methanol synthesis from CO_2 hydrogenation over La–M–Cu–Zn–O (M = Y, Ce, Mg, Zr) catalysts derived from perovskite-type precursors, J. Power Sources 251 (2014) 113–121.
[48] R.D.l.P.P. Toyir J., Fierro J. L. G. and Homs N., Catalytic Performace for CO_2 Conversion to Methanol of Gallium Promoted Copper based Catalysts: Influence of Metallic Precursors, Appl. Catal. B, 34 (2001) 255-266.
[49] C. Zhong, X. Guo, D. Mao, S. Wang, G. Wu, G. Lu, Effects of alkaline-earth oxides on the performance of a CuO-ZrO_2 catalyst for methanol synthesis via CO_2 hydrogenation, RSC Adv. 5 (2015) 52958–52965.
[50] P. Gao, F. Li, H. Zhan, N. Zhao, F. Xiao, W. Wei, L. Zhong, H. Wang, Y. Sun, Influence of Zr on the performance of Cu/Zn/Al/Zr catalysts via hydrotalcite-like precursors for CO_2 hydrogenation to methanol, J. Catal. 298 (2013) 51–60.